JOURNAL OF CATALYSIS 125, 207–213 (1990)

Morphology Studies of MnO_x-Modified Ni(111) Surfaces by Scanning Tunneling Microscopy

YONG-BO ZHAO, TZER-SHEN LIN, AND YIP-WAH CHUNG

Department of Materials Science and Engineering, and Center for Catalysis and Surface Science, Northwestern University, Evanston, Illinois 60208

Received January 9, 1990; revised March 28, 1990

Morphology of clean Ni(111) and MnO_x (x between 0.2 and 0.5)-modified Ni(111) surfaces has been studied by scanning tunneling microscopy (STM) under ultrahigh vacuum conditions. Oxide islands were clearly observed. The nickel-oxide perimeter site concentration was measured as a function of oxide coverage and was found to correlate very well with results from earlier CO thermal desorption studies of the same system. These results strongly suggest the importance of perimeter sites in systems exhibiting strong metal–support interaction. © 1990 Academic Press, Inc.

INTRODUCTION

Strong metal–support interaction (SMSI), which is characterized by suppression of CO and H_2 chemisorption (*1–8*), as well as by a change in activity and selectivity toward certain reactions (*4, 9–15*), has been the subject of many studies in the last decade. Current evidence indicates that SMSI is largely the result of migration of reduced support species onto the metal surface (*16–19*).

When a metal surface is partially covered by reduced oxide islands, there are three types of surface sites: uncovered metal sites, oxide sites, and perimeter sites between the two. Suggestions have been made that new active sites could be created at the metal–oxide interface which are responsible for the enhanced CO hydrogenation activity (*6, 20*). Previous results of CO chemisorption studies on MnO_x/Ni(111) (*21*) and AlO_x/Ni(111) (*22, 23*) model catalysts showed a new CO adsorption state, as evidenced by the lower desorption temperature and lower C–O stretching frequency, which was attributed to CO adsorption at or near the metal–oxide perimeter sites (*21–23*). Since weakened C–O bonding would accelerate CO dissociation, and weakened carbon-surface bonding would accelerate hydrocarbon desorption, these perimeter sites are believed to be the new active sites in SMSI. Such perimeter-site-related enhancement of CO hydrogenation activity has been observed in TiO_x/Pt (*24*) and TiO_x/Rh (*25*).

At a given average oxide coverage, the concentration of perimeter sites is determined by the oxide morphology. That is, the perimeter site concentration is a function of the size and shape of these surface oxide islands. We made an attempt to use STM to image a clean Ni(111) surface and the same surface partially covered with MnO_x species (*22*). The results were quite encouraging: STM images showed a distinct difference between the smooth surface of clean Ni(111) and the island-like features from the MnO_x/Ni(111) surface (*22*). The main drawback of that experiment was that the imaging was done in air.

In order to avoid any unnecessary ambiguity in exposing the specimen to air, a UHV scanning tunneling microscope was constructed and incorporated into an existing UHV surface analysis system. The present study attempts to examine the surface morphology of Ni(111) with different MnO_x coverages, in particular the perime-

0021-9517/90 $3.00

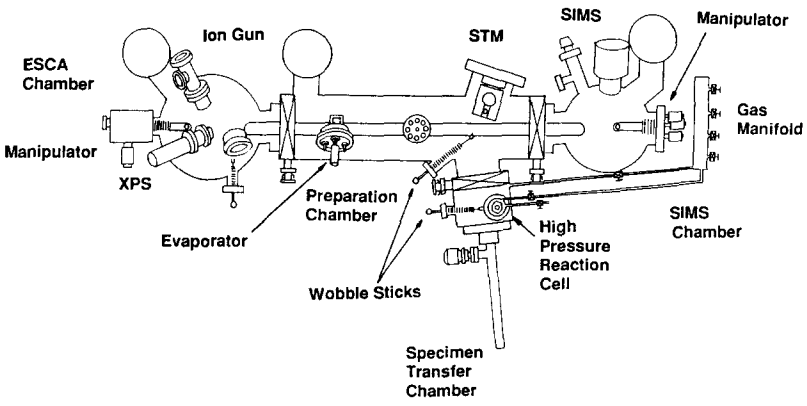

FIG. 1. Schematic diagram of VG Scientific ESCA/SIMS UHV chamber.

ter length of oxide islands as a function of oxide coverage.

EXPERIMENTAL

Experiments were carried out in a VG Scientific ESCA/SIMS chamber. In order to accomplish the present study, we added a metal/oxide evaporator, which was identical to that used in previous CO chemisorption experiments (*21–23*), and a UHV-compatible scanning tunneling microscope. A schematic diagram of the UHV chamber is shown in Fig. 1. The scanning tunneling microscope used in this work is based on a piezoelectric tube scanner and is mounted on a standard 8-in. conflat flange. Figure 2 shows a schematic diagram of the microscope. During experiments, the ESCA chamber, SIMS chamber, and preparation chamber were all maintained in the 10^{-10} Torr range. The specimen used in these experiments was the same Ni(111) single-crystal disk used in previous CO chemisorption studies. It is about 1 cm^2 in surface area and 1 mm in thickness. The specimen transfer facility in the preparation chamber allowed the specimen to be transferred between various chambers without breaking the vacuum.

In the experiments, the specimen was first purged of bulk impurities by a series of Ar ion sputtering and high-temperature annealing cycles. This was followed by an oxidation–reduction cycle at 773 K to remove the residual surface carbon. The evaporation source was MnO_2 powder held in a Ta boat. During the evaporation, the boat was heated to about 800 K with the Ni crystal held at room temperature. Separate X-ray photoemission experiments showed that such a procedure resulted in a surface oxide with an oxygen-to-manganese atomic ratio close to one. The oxygen-to-manganese ratio was calibrated using the sensitivity data from the VG XPS Data Pool. The surface was then reduced at 773 K in H_2 for 10 to 15 min. This produced an unoxidized smooth nickel surface (*21*). The oxygen-to-manganese ratio after reduction was between 0.2 and 0.5. XPS was used to verify that the

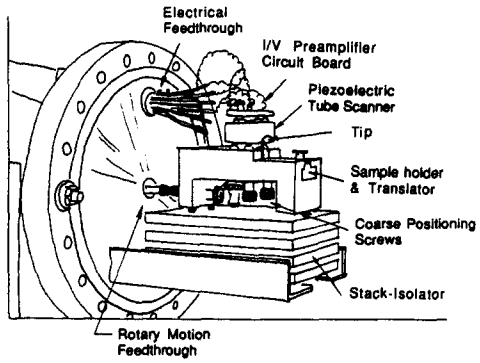

FIG. 2. Schematic diagram of the UHV-compatible STM setup.

surface was clean after each step of preparation. After a surface was prepared, the specimen was allowed to cool to room temperature before being examined by the scanning tunneling microscope.

STM measurements were done using a sharp Pt/Ir tip in the constant current mode at 1.3 nA and a sample bias of +30 mV relative to the tip. Five to fifteen images from different parts of the surface were taken for each oxide coverage. The actual oxide coverage and the perimeter length of oxide islands per unit area (Ni + MnO_x) were then determined after each oxide deposition.

RESULTS AND DISCUSSIONS

Figure 3 shows an STM topographic image of a clean Ni(111) surface after annealing at 773 K. The scanned area was 630 × 630 Å^2. One can see terraces with widths of about 100 to 200 Å separated by monatomic and diatomic steps.

After the oxide deposition and subsequent high-temperature reduction, the MnO_x-modified Ni(111) surfaces were examined by STM. Compared with the clean nickel surface, the oxide-covered surfaces appear to generate more noise or current spikes during imaging. This might be due to electronic trapping effects in the partially reduced oxide-covered surface, as has been reported by Koch and Hamers (*26*). Figure 4a shows a 79 × 79 Å^2 area of a Ni(111) surface with an average oxide coverage of 0.35 monolayer. Figure 4b shows a similar 320 × 320 Å^2 scan with an average oxide coverage of 1.3 monolayers. Such gray-scale images clearly reveal the existence of patches on the surface evolving with oxide deposition. This STM setup is currently not capable of distinguishing between manganese oxide and nickel regions. However, the work function difference between manganese oxide and nickel should not be large enough to bring about apparent height variations greater than 1 Å. Under our circumstances, we expect topography to dominate in STM images. The fact that the size and height of these patches increase with increasing manganese oxide coverage is consistent with our image interpretation.

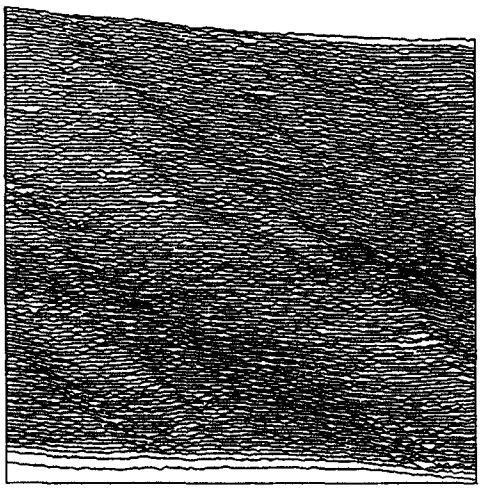

FIG. 3. STM image of a Ni(111) surface after sputter-anneal and oxidation–reduction treatment. The area is 630 × 630 Å^2. The height variation over the entire image is about 10 Å.

Based on the above argument, we attribute the observed patches as surface oxide islands. The oxide perimeter length per unit area of the specimen as well as the actual oxide coverage were then measured from these STM images. Figure 5 shows the oxide perimeter site length per unit area of MnO_x/Ni(111) surfaces as a function of the average oxide coverage. The vertical scale on the right-hand side gives perimeter length per unit area in 1/Å.

Our previous CO thermal desorption study of the MnO_x/Ni(111) surface showed a 305 K TDS peak, which we assigned to CO adsorbed at the perimeter site (*21*). As a comparison, the area under the 305 K CO thermal desorption peak has been converted into number of CO molecules per unit area (vertical scale of 10^{14}/cm^2 on the left-hand side), and the result was then superimposed on the STM data in Fig. 5. To convert the TDS data into CO concentration, we used the area under the 415 K CO thermal desorption peak from a clean Ni(111) surface after saturation CO expo-

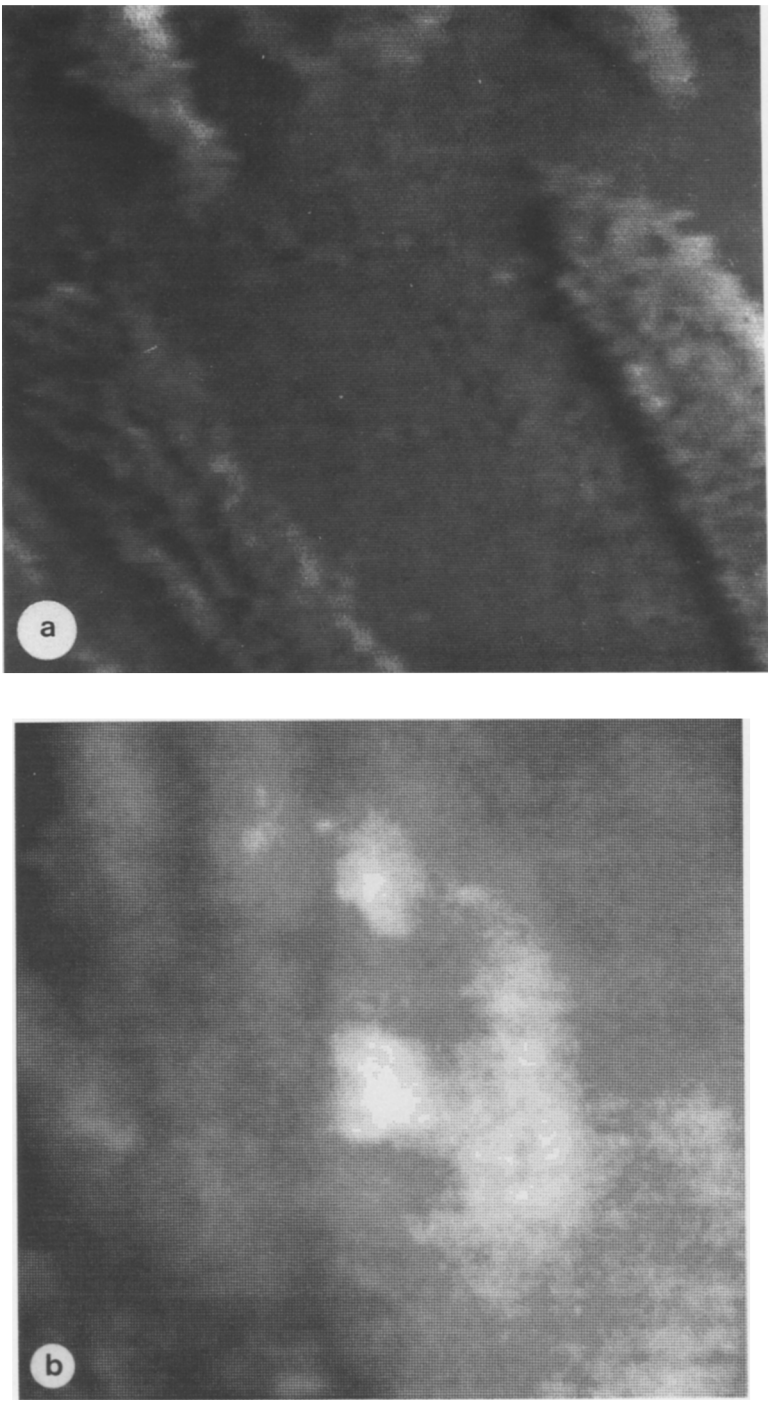

FIG. 4. (a) STM image of an MnO_x-covered Ni(111) surface. The scanned area is 79 × 79 Å^2. The average oxide coverage is 0.35 ml. The height difference between the highest (brightest) and lowest (darkest) part of the image is about 5 Å. (b) STM image of an MnO_x-covered Ni(111) surface. The scanned area is 320 × 320 Å^2. The average oxide coverage is 1.3 ml. The maximum height difference is about 5 Å.

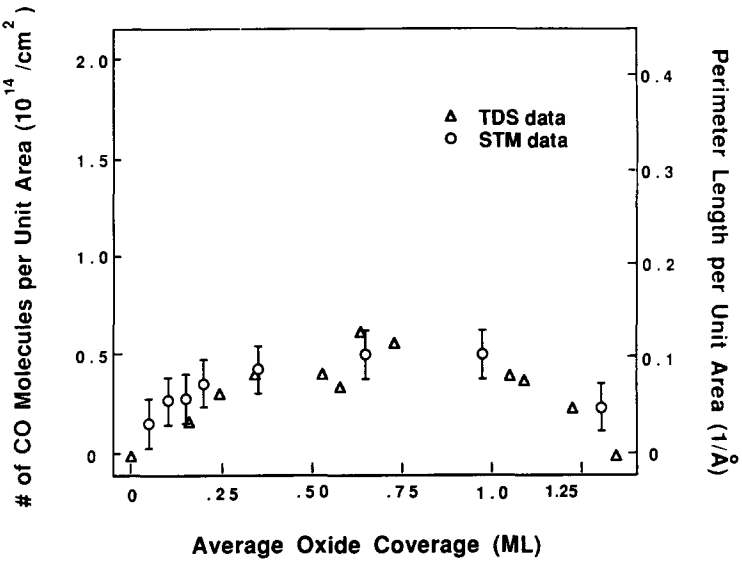

FIG. 5. Superimposed (△) CO thermal desorption and (○) STM results from MnO_x/Ni(111). For the TDS results, the area under the 305 K peak is converted into the number of CO molecules per square centimeter (the vertical scale on the left-hand side) and plotted as a function of average oxide coverage. For the STM results, the measured oxide perimeter length per unit area of the specimen surface (1/Å) is plotted as a function of average oxide coverage (the vertical scale on the right-hand side).

sure as reference (9.3×10^{14} CO molecules/cm^2). From Fig. 5, one can see that the perimeter site concentration measured from the STM varies in a manner similar to that of the 305 K TDS data.

As can be seen from Fig. 5, the maximum oxide perimeter length per unit area is (0.10 ± 0.02)/Å or $(1.0 \pm 0.2) \times 10^7$ cm/cm^2. With a nearest-neighbor distance of 2.49 Å for Ni, this corresponds to $(4.0 \pm 0.8) \times 10^{14}$ Ni atoms/cm^2 along the perimeter. Given the fact that the primary CO adsorption sites on Ni(111) are twofold bridge sites, this implies that there are $(4.0 \pm 0.8) \times 10^{14}$ possible CO adsorption sites on the perimeter per square centimeter. But not all twofold sites are occupied by CO. When one examines the surface unit cell for adsorbed CO on Ni(111) at saturation coverage (Fig. 6), one can show by direct counting that there is one adsorbed CO every six twofold bridge sites. Therefore, the maximum concentration of CO adsorbed on Ni atoms around the oxide perimeter is simply equal to $(6.7 \pm 1.3) \times 10^{13}$/cm^2. This compares very well with the maximum CO surface concentration corresponding to the 305 K desorption peak (about 6×10^{13}/cm^2, from Fig. 5). One such oxide island is

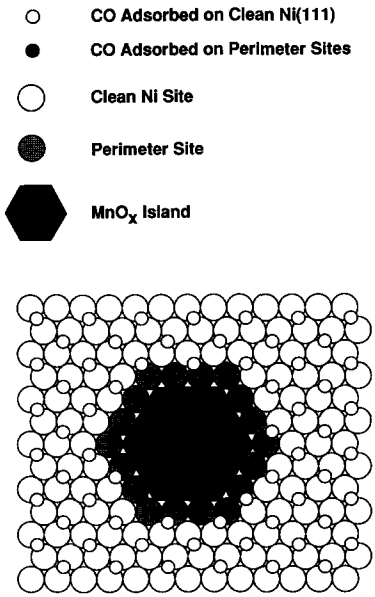

FIG. 6. Schematic diagram of CO adsorption on a partially covered Ni(111) surface.

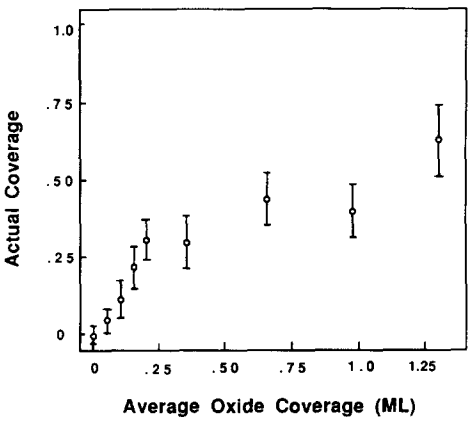

FIG. 7. Actual oxide coverage measured by STM vs average oxide coverage determined by quartz crystal thickness monitor.

shown in Fig. 6 with adsorbed CO on perimeter sites to show this geometric effect.

The above results reveal that even under optimum conditions, less than 4% (6.7×10^{13} divided by 1.9×10^{15}, number of Ni atoms per unit area of Ni(111) surface) of the entire surface can be attributed to perimeter sites. If we assume these perimeter sites to be the new active sites in CO hydrogenation when the catalyst is in the SMSI state (*21, 22*), only a small fraction of the surface metal sites constitute active sites for the reaction, consistent with early CO hydrogenation results (*4, 6, 12*).

Figure 7 shows the actual oxide coverage from STM measurements versus the average oxide coverage determined by the quartz crystal thickness monitor. For coverage $\leq 1/3$ monolayer, the actual coverage increases linearly with average coverage. This is consistent with our previous results, which showed that the amount of CO adsorbed on Ni(111) surface decreased almost linearly with increasing MnO_x coverage (*21*). It implies that the suppression of CO chemisorption is due mainly to the physical blockage of surface metal sites by the oxide overlayer. However, the deviation of STM-measured oxide coverage from the average coverage becomes substantial as the coverage increases, signifying the growth of three-dimensional oxide islands.

CONCLUSIONS

The present STM study of MnO_x-modified Ni(111) surface morphology proved that reduced MnO_x surface species form three-dimensional islands. The MnO_x-Ni perimeter site concentration has been measured from STM data as a function of the average oxide coverage, which correlates very well with previous work on CO thermal desorption. This adds further evidence that the perimeter sites in SMSI systems are primarily responsible for enhanced CO hydrogenation activities.

ACKNOWLEDGMENTS

Acknowledgment is made to the Donors of the Petroleum Research Fund, administered by the American Chemical Society, for support of this research. This work is also partly supported by the Center for Engineering Tribology at Northwestern University.

REFERENCES

1. Tauster, S. J., Fung, S. C., and Garten, R. L., *J. Amer. Chem. Soc.* **100** 170 (1978).
2. Tauster, S. J., and Fung, S. C., *J. Catal.* **55,** 29 (1978).
3. Baker, R. T., Prestridge, E. B., and Garten, R. L., *J. Catal.* **59,** 293 (1979).
4. Vannice, M. A., Wang, S. Y., and Moon, S. H., *J. Catal.* **71,** 152 (1981).
5. Kao, C. C., Tsai, S. C., and Chung, Y. W., *J. Catal.* **73,** 136 (1982).
6. Burch, R., and Flambard, A. R., *J. Catal.* **78,** 389 (1982).
7. Santos, J., Phillips, J., and Dumesic, J. A., *J. Catal.* **81,** 147 (1983).
8. Hicks, R. F., Yen, Q. J., and Bell, A. T., *J. Catal.* **89,** 498 (1984).
9. Vannice, M. A., and Garten, R. L., *J. Catal.* **56,** 236 (1979).
10. Wang, S. Y., Moon, S. H., and Vannice, M. A., *J. Catal.* **71,** 167 (1981).
11. Meriaudeau, P., Ellestad, O. H., Dufaux, M., and Naccache, C., *J. Catal.* **75,** 243 (1982).
12. Vannice, M. A., and Twu, C. C., *J. Catal.* **82,** 213 (1983).
13. Erdohelyi, A., and Solymosi, F., *J. Catal.* **84,** 446 (1983).
14. Hicks, R. F., and Bell, A. T., *J. Catal.* **90,** 205 (1984).
15. Jiang, X. Z., Hayden, T. F., and Dumesic, J. A., *J. Catal.* **83,** 168 (1985).

16. Resasco, D. E., and Haller, G. L., *J. Catal.* **82,** 279 (1983).
17. Ko, C. S., and Gorte, R. J., *J. Catal.* **90,** 59 (1984).
18. Takatani, S., and Chung, Y. W., *Appl. Surf. Sci.* **19,** 341 (1984).
19. Dwyer, D. J., Caneron, S. D., and Gland, J., *Surf. Sci.* **159,** 430 (1985).
20. Vannice M. A., and Sudhakar, C., *J. Phys. Chem.* **88,** 2429 (1984).
21. Zhao, Y. B., and Chung, Y. W., *J. Catal.* **106,** 369 (1987).
22. Zhao, Y. B., Lin, T. S., and Chung, Y. W., *Mater. Res. Soc. Symp. Proc.* **111,** 435 (1988).
23. Zhao, Y. B., PhD thesis, Northwestern University (1988).
24. Demmin, R. A., Ko, C. S., and Gorte, R. J., *in* "Strong Metal–Support Interactions," ACS Symposium Series Vol. 298, p. 48. Amer. Chem. Soc., Washington, DC 1986.
25. Levin, M. E., Salmeron, M., Bell, A. T., and Somorjai, G. A., *J. Catal.* **106,** 401 (1987).
26. Koch, R. H., and Hamers, R. J., *Surf. Sci.* **181,** 333 (1987).